ACS Sustainable Chemistry & Engineering

Research Article

pubs.acs.org/journal/ascecg

Influence of Surface Structure on the Capacity and Irreversible Capacity Loss of Sn-Based Anodes for Lithium Ion Batteries

Li Li,*[,†,§] Xuan Liu,[‡] Shulan Wang,*[,†] and Wenzhi Zhao[†]

[†]Department of Chemistry, School of Science, Northeastern University, Shenyang 110819, China

[‡]Department of Materials Science and Engineering, Carnegie Mellon University, Pittsburgh, Pennsylvania 15213, United States

[§]Department of Materials Science and Engineering, Cornell University, Ithaca, New York 14853, United States

ABSTRACT: The lithium ion battery is viewed as one of the most important energy storage devices for sustainable transport of power, and it is now attracting tremendous attention. In the present work, dense Sn films were pulse electrodeposited on a Cu substrate and then post-treated at 200 °C under different conditions, including electroplating a Cu coating film and heat treatment in different atmospheres. Surface morphology and composition of the films were characterized by scanning electron microscopy, X-ray diffraction, and energy dispersive spectroscopy. These films were then assembled as anodes for Li ion batteries with their electrochemical properties investigated. The Sn-based anode with a Cu coating post-heated in argon for 12 h forms a surface with Cu_6Sn_5/Sn as the primary phase. It showed the largest first cycle charge/discharge capacity and highest irreversible capacity loss (IRC). The Sn-based anode sintered in air for 48 h was surface modified by SnO and showed the smallest IRC. Change in charge/discharge capacities as well as IRC at different cycles was also analyzed with the architecture of multi-layered anodes. Defects in the Cu_6Sn_5/Sn surface phase lead to an increase in both the first cycle capacity and IRC of the anode, while the existence of SnO is beneficial to the decrease in the first cycle IRC of the anode. This work provides a fundamental understanding for the influence of the surface morphology, composition, and microstructure of Sn-based anodes on their electrochemical performances.

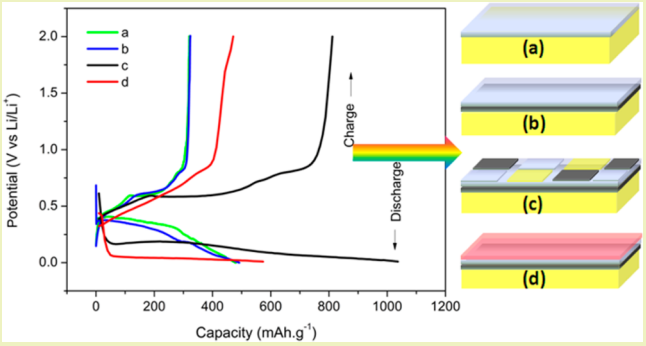

KEYWORDS: *Electrochemistry, Li ion battery, Capacity, Irreversible capacity loss, Sn*

INTRODUCTION

Currently, sustainable clean energy is widely studied to replace conventional fossil fuel that has placed great pressure on the environment because of greenhouse gas emissions.[1−5] Numerous solar and wind power energy plants have been invested in to exploit sustainable and renewable energy.[6] The lithium ion battery is considered one of the most potential candidates for sustainable transport of power from green energy power plants.[7,8] The most commonly used graphite anode for lithium ion batteries suffers from low energy density and safety issues.[9,10] Sn-based anodes are considered promising candidates to replace the graphite anode in lithium ion batteries because of their high gravimetric and volumetric capacity.[10−12] As a result, the improvement in their charge/discharge properties and cycle performances is of great technical interest and scientific significance.[13−17] One major challenge restricting the application of Sn anodes in lithium ion batteries is their large irreversible capacity loss (IRC) at the first charge/discharge cycle.[10,18−20] Extra Li needs to be provided for compensation of the lost capacity, decreasing the energy density of the battery. The IRC can be caused by multiple factors, such as the loss of electrical connection between active materials due to their large volume change during cycling,[10,21,22] formation of a passive solid−electrolyte interface (SEI) film via the lithium reaction with the electrolyte,[23−27] trapping of Li in the host alloy,[28−31] and formation of non-deintercalation Li_2O between Li and the surface oxide layer.[32,33]

The IRC of Sn-based anodes is strongly dependent on the particle size, composition, and preparation methods of active materials. Sn-based oxide materials, such as SnO, SnO_2, Li_2SnO_3, and $SnSiO_3$, showed IRC values ranging from 200 to 700 mAh g^{-1}.[13] Sn-riched La−Co−Sn ternary alloys, prepared by the arc-melting process with subsequent ball milling, had IRC values of ∼400 mAh g^{-1} and showed a slight increase in IRC value with increase in ball-milling time.[34] The thin film Sn anode prepared by electroplating (a few micrometers in thickness) had an IRC value of ∼40 mAh g^{-1},[22] whereas nanosized Sn[33,35] and SnSb alloys[32,33] showed IRC values of 250−500 mAh g^{-1}. Cu_6Sn_5 surface-modified Sn anodes prepared by electrodepositing and post-heat treatment had IRC values of 270 mAh g^{-1}.[36]

Received: March 20, 2014
Revised: May 15, 2014
Published: May 19, 2014

Currently, understanding of the IRC values for improvement in the electrochemical performance of Sn-based anodes has attracted extensive attention from the scientific community. Wachtler et al. studied the IRC values of a Sn/SnSb anode by analyzing the galvanostatic cycling behavior in different electrolytes.[32] In the work by Wang et al., electrochemical impedance spectroscopy (EIS) was used to investigate the contact resistance of the sandwiched electrode (Sn, $Li_{4.4}Sn$, and $AlSi_{0.1}$) and electrochemical kinetics during the initial lithium insertion.[35] Their result showed that the increase in contact resistance is caused by both SEI film formation and active materials pulverization.[35] The study by Huang et al. on the SnZn alloy anode via the first-principle plane wave pseudopotential method indicated that the dead lithium phase $Li_xSn_4Zn_{8-(4-x)}$ (x = 4.74, 7.72) led to irreversible capacity loss of the battery because of its high formation energy.[37]

Our previous work has shown a strong influence of the electrochemical performance of Sn-based three-layer anode by its layer structure.[38] However, the role of surface physical parameters, which is a necessity for design of high performance anodes for lithium ion batteries, is still unknown for the Sn-based layered structure. Herein, the Sn films were treated with different conditions to obtain multi-layered anodes with different architectures. Detailed analysis was used to investigate the influence of surface morphology, composition, and microstructure on their capacity and IRC at different cycles. The result showed that the capacity and IRC of Sn-based anodes strongly depend on their surface properties. Presence of defects in active material Cu_6Sn_5/Sn leads to an increase in both the first cycle capacity and IRC, while the presence of SnO causes a decrease in first cycle IRC. The relationship between IRC as well as the first cycle charge/discharge capacity and their structural factors of the Sn-based anodes is revealed in detail. The major contribution of the current work is to improve the fundamental understanding of the influences of surface morphology, composition, and structure on the electrochemical performances of multi-layered anodes, which is beneficial for engineering the design of such layered anodes.

EXPERIMENTAL SECTION

Sn-based thin films were fabricated via electrodeposition with commercial Cu foils as the substrate. The electrodeposition was conducted in a three electrode cell (EG&G PAR273A) with Cu foils as the working electrode, Pt (1 cm^2 in area) as the counter electrode, and saturated calomel as the reference electrode. Pulse currents and time intervals were set to be 15 mA, 2.0 s and −1 mA, 0.5 s, respectively. The corresponding current densities are 3.75 and 0.23 mA cm^{-2}. The detailed experimental setup is reported previously.[36,38] The active material in the anode was measured to be around 4.6 mg. A control sample was fabricated by further electrodepositing Cu after electrodepositing Sn film from the aqueous solution composed of 0.1 mol L^{-1} $CuCl_2$ and 0.16 mol L^{-1} $Na_3C_6H_5O_7$ at the same pulse currents and time intervals for 600 s. The films were then sintered at 200 °C in argon or air from 12 to 48 h in a semi-sealed quartz tube (65 mm × 50 mm × 600 mm). The detailed experimental conditions for the samples used in the experiment are shown in Figure 1.

The phase composition of Sn-based film was analyzed by X-ray diffraction (XRD) using a Philips PW3040/60 diffractometer at a scanning rate of 0.03° min^{-1} for 2θ in the range of 25 to 85°. Scanning electron microscopy (SEM, SSX-550) was used to characterize the surface morphology of the films at an accelerating voltage of 30 kV. Energy dispersive X-ray spectroscopy (EDX) (Oxford INCA) equipped in the SEM was used to analyze the cross-sectional element distribution of thin films.

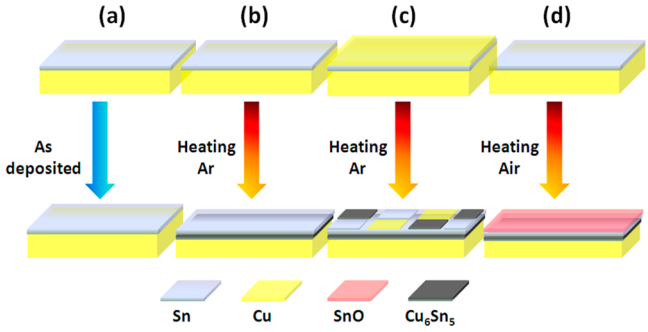

Figure 1. Schematic of experiment conditions for different samples: (a) as-electrodeposited (denoted as sample a), (b) sintered at 200 °C in argon for 12 h (denoted as sample b), (c) covered by Cu and then sintered at 200 °C in argon for 12 h (denoted as sample c), and (d) sintered at 200 °C in air for 48 h (denoted as sample d).

The Sn-based films were then cut into circles (6.5 mm in diameter) and assembled as anodes for Li ion coil cells (CR2025 type) in a Labstor glovebox, with Li and lithium hexafluorophosphate as the cathode and electrolyte, respectively. The charge/discharge performance of the cell was recorded using the cell test instrument (LAND CT2001A) in the potential range of 0.01− 2.0 V (vs Li/Li^+) with a constant current of 3 mA. AC impedance spectra of the cells were measured by an EG&G PAR273A potentiostat/galvanostat and a 5210 Lock-in Amplifier, with a frequency range and ac amplitude from 100 mHz to 100 Hz and 5 mV, respectively. The ac impedance spectra were then simulated to obtain the equivalent circuit parameters with Zview software.

RESULTS AND DISCUSSION

Figure 2 shows the X-ray diffraction patterns of Sn-based films. Shown in Figure 2a and b, peaks of the as-electrodeposited film (sample a) and the sintered film (sample b) can be indexed as metallic Sn (JCPDS 01-086-2264). The corresponding peaks

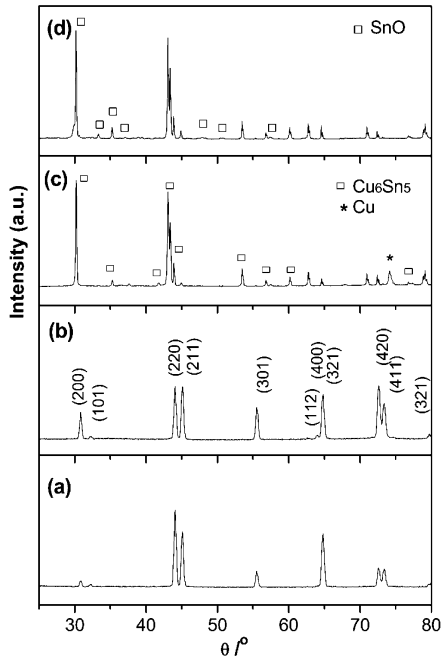

Figure 2. X-ray diffraction patterns of Sn-based films: (a) as-electrodeposited, (b) sintered at 200 °C in argon for 12 h, (c) covered by Cu and then sintered at 200 °C in argon for 12 h, and (d) sintered at 200 °C in air for 48 h.

are marked in the figure. No other phase was observed. It is reasonable to assume that the bimetallic Cu_6Sn_5 phase may exist in the interface between the Sn film and Cu substrate because of the strong diffusivity of Cu.[39,40] The heat treatment should promote the diffusion of Cu into the Sn film.[39] That no Cu_6Sn_5 peaks were observed can be ascribed to a negligible amount of Cu−Sn bimetallics or that the thickness of the Sn film exceeded the penetration depth of X-ray. The enhanced intensity of some diffraction peaks of the sintered film (Figure 2b) is attributed to the increase in crystallinity of metallic Sn after heat treatment. The average crystallite size of Sn is calculated to be 0.5 μm based on the Scherrer equation.[41] The XRD spectra of the Sn film sintered at 200 °C in argon for 12 h with a Cu coating is shown in Figure 2c. Its primary phases are Sn and bimetallic Cu_6Sn_5 (JCPDS 03-065-2303). Peaks related to the Cu phase indicate that the top Cu layer has not been completely converted into Cu_6Sn_5. The XRD result of the Sn-based film sintered at 200 °C in air for 48 h is presented in Figure 2d. In addition to Sn and Cu_6Sn_5, the presence of SnO is confirmed because of oxidation of Sn in the top layer during heat treatment.

Surface and cross-sectional images of the Sn-based films treated under different conditions are presented in Figure 3. The as-electrodeposited Sn film consists of large Sn crystals with sizes of 5−10 μm and thicknesses of 10−13 μm (Figure 3a,b). Very little amounts of Cu−Sn intermetallics are observed at the interface between the Sn film and Cu substrate. Sintering at 200 °C in argon for 12 h does not apparently change the surface morphology of the Sn film, but the intermetallic layer is widened between the Sn film and Cu substrate (Figure 3c,d). Intermetallic Cu_6Sn_5 can be confirmed according to the atomic weight percentage of Cu and Sn in the EDX result shown in Figure 3d. The surface morphology of the Sn-based film with a Cu coating and post-heated in argon for 12 h (Figure 3e) significantly differs from the above two anodes. Its rough surface is composed of small grains, which are beneficial for the insertion/extraction of Li ions. A complicated layered structure (Figure 3f) was formed for the anode. Intermetallic Cu_6Sn_5 was produced both on the outermost layer and inner layer adjacent to the Cu substrate. Consistent with the XRD result shown in the earlier section, the surface layer is primarily composed of a mixture of Sn and Cu_6Sn_5. The surface morphology of the sample annealed at 200 °C in air for 48 h did not have an apparent change. Its three-layer architecture consists of SnO as the top layer, Sn as the middle layer, and Cu_6Sn_5 as the bottom layer, with thicknesses of 0.5, 3.2, and 4 μm, respectively, as shown in our previous work.[38]

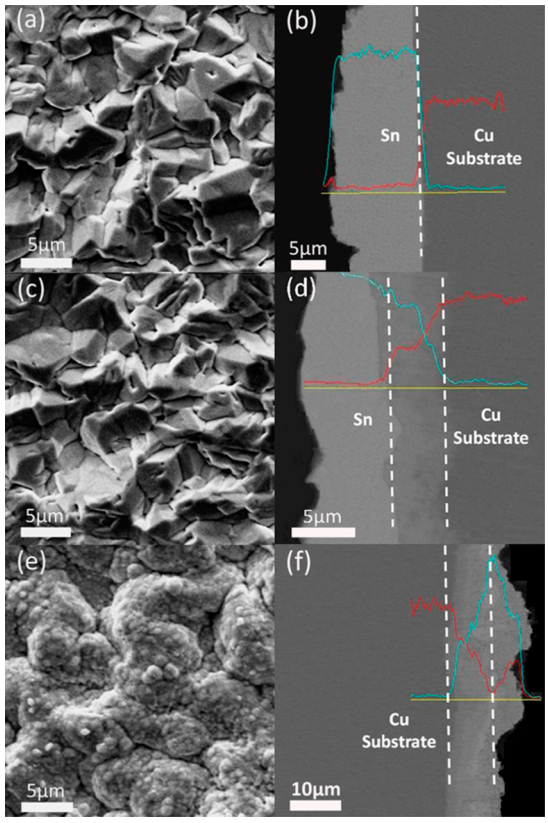

Figure 3. Surface morphology and cross-sectional images of Sn-based films: (a,b) as-electrodeposited, (c,d) sintered at 200 °C in argon for 12 h, and (e,f) covered by Cu and then sintered at 200 °C in argon for 12 h. The elemental analyses represented as different color curves are presented in the figure (red, signal from Cu; blue, signal from Sn).

The potential profiles of different Sn-based film anodes in the first charge/discharge cycle are presented in Figure 4. It can be

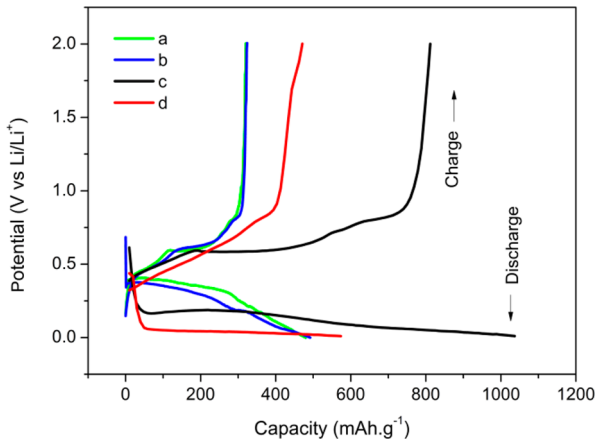

Figure 4. Potential profiles of Sn-based films treated under different conditions for the first charge/discharge cycle: (a) as-electrodeposited, (b) sintered at 200 °C in argon for 12 h, (c) covered by Cu and sintered at 200 °C in argon for 12 h, and (d) sintered at 200 °C in air for 48 h.

observed that the charge curves of the as-electrodeposited anode (Figure 4a) and the anode heat treated in argon (Figure 4b) nearly coincide with each other. Both anodes have the same first cycle charge/discharge capacity and two charge platform potentials of 0.65 and 0.81 V. The only difference lies in the discharge potential, the value of which is slightly lower for the heat-treated anode. The result indicates that the first cycle charge/discharge capacity of the dense Sn anode is dependent primarily on its surface morphology and composition and scarcely on its bulk structural property.

The Cu_6Sn_5 surface-modified anode (Figure 4c) shows the largest first cycle charge/discharge capacity and platform potential. Its charge/discharge capacity reaches 725 and 1036.7 mAh g^{-1}, respectively. The discharge capacity exceeds the theoretical value of Sn (997 mAh g^{-1}). Induced by the chemical driving force and thermal stress,[42] Cu atoms in the surface were squeezed and diffused into the underneath Sn layer during heat treatment. The structural changes and thermal activation can induce intrinsic structural defects.[43] Those energetically favorable and thermodynamically instable defects

can influence the electrochemical kinetics during Li extraction[44] and are favorable for diffusion of Li ions.[45]

Compared with that of the as-electrodeposited Sn anode (Figure 4a), the first cycle charge/discharge capacity of SnO surface-modified anode (treated at 200 °C in air for 48 h) (Figure 4d) increases to 472/574 mAh g^{-1}. SnO is reduced first and then alloyed/dealloyed by the following two steps[46]

$$SnO + 2Li^+ + 2e^- \rightarrow Li_2O + Sn \quad (1)$$

$$Sn + xLi^+ + xe^- \Leftrightarrow Li_xSn \quad (2)$$

Step 1 has two balanced effects on the capacity of the anode. The presence of SnO provides an extra charge capacity. On the other hand, the formation of non-deintercalation Li_2O leads to an increase in internal resistance of the anode, which can consequently lead to incomplete delithiation with some Li ions trapped and remaining in active particles,[20,22−25] decreasing the first cycle discharge capacity of the cells. In addition, Sn produced in step 1 is immediately consumed in step 2 before growing into larger crystals. This can also accelerate step 2 and increase the discharge capacity.

Table 1 lists the first cycle charge/discharge capacities and the corresponding IRC values of the Sn-based anodes. The Sn anode before (sample a) and after (sample b) heat treatment in argon shows similar charge/discharge capacities and IRC values. The heat treatment at 200 °C in argon for 12 h has little influence on the IRC values of Sn-based anodes. The Sn-based anode with Cu_6Sn_5 surface modification (sample c) shows the largest IRC value (311.7 mAh g^{-1}) among all the anodes.

Table 1. First Cycle Charge/Discharge Capacities and IRC Values of Sn-Based Anodes for Li Ion Cells[a]

sample no.	charge capacity (mAh g^{-1})	discharge capacity (mAh g^{-1})	IRC (mAh g^{-1})
a	350.5	479.6	129.1
b	353.8	489.6	135.8
c	725	1036.7	311.7
d	472.1	574.2	102.1

[a](a) as electrodeposited, (b) sintered at 200 °C in argon for 12 h, (c) covered by Cu and then sintered at 200 °C in argon for 12 h, and (d) sintered at 200 °C in air for 48 h.

The high IRC value of sample c may be attributed to its large contacting area of the surface with electrolytes and thus formation of a thick SEI film. Another reason for the high IRC value may lie in the formation of intrinsic defects induced by structural changes and thermal activation as discussed above. Li ions are easily trapped in those energetically favorable and thermodynamically instable defects in the surface-modified layer,[10,47−49] resulting in high IRC values.

The first cycle charge/discharge capacity of the SnO surface-modified anode (sample d) was increased by 34.7% and 19.7%, compared with that of the as-electrodeposited anode (sample a). This increase in capacity is accompanied by a decrease in the IRC value to 102.1 mAh g^{-1}. The presence of the surface SnO layer increases the charge capacity by the reaction in step 1 and the formation of non-deintercalation Li_2O have a negative influence on the increase of discharge capacity to some extent, resulting in a decrease in the IRC values. It is reported that coating of the SnO_x film can prevent formation of SEI films.[50,51]

The cyclic performance of Sn-based film anodes treated under different conditions for Li ion batteries were measured for 50 cycles at the voltage of 0.01−2.0 V (vs Li/Li^+) and at the constant current of 3 mA. Corresponding results are presented in Figure 5. The IRC curves of the anodes are also shown in Figure 5. It should be noted that the charge/discharge curves in different cycles can be divided into different regions, which are related to the layered structure of the fabricated anodes. The charge/discharge capacity of the as-electrodeposited Sn (shown in Figure 5a) shows a peak value of 331.3/323.3 mAh g^{-1} at the 14th cycle because of its dense structure. The thick and dense Sn anode with large crystallite size limits the diffusion of Li ions for alloying reaction. It is important to note that the charging process stops automatically as the potential increases to the set value of 2.0 V. As a result, Sn in the anode is only partially involved in the charge/discharge process in a single cycle initially. The Sn anode gradually becomes porous during the repeated charging/discharging processes, while more and more active Sn materials in the inner layer participate in the lithiation/delithiation process. In other words, the capacity increases with an increasing insertion depth of Li in the anode. Cracking of active materials caused by the volume change leads to fading of the capacity after repeated cycles.

The Sn anode heated in an argon atmosphere for 12 h as presented in Figure 5b shows a similar cyclic performance to that of the as-electrodeposited Sn anode, but it achieves its maximum charge capacity in the 10th cycle. The IRC values of the heated anode in different cycles are also slightly lower than those of the as-electrodeposited anode. This is likely a result of a decrease in stress in the anode during heat treatment and less SEI film production.

The cyclic curve of the Cu_6Sn_5 surface-modified anode (shown in Figure 5c) can be categorized as two different regions. Peak values are observed for charge/discharge capacities and IRC values in the fourth and fifth cycles, respectively. The surface layer is primarily composed of Cu_6Sn_5 and Sn. The concentration of Sn reaches a maximum between the surface Cu_6Sn_5 layer and the internal layer (shown in Figure 3f). The Sn layer acts as an active matrix buffer to alleviate the volume change in the active materials,[52] which accounts for the peak value of the charge/discharge capacity at the fourth cycle. However, the active matrix has disadvantages of low reversibility and strong dependence on the charge depth.[53,54] Therefore, the high IRC value in the fifth cycle indicates that the lithium/delithum reaction has penetrated through the Sn layer. The charge/discharge capacity is maintained at a value of around 520 mAh g^{-1} within the further 10 cycles, in correspondence to the capacity of the inner Cu_6Sn_5 layer in the anode. The alloying reaction of Cu_6Sn_5 with Li can be expressed as follows[55]

$$10Li^+ + Cu_6Sn_5 + 10e^- \Leftrightarrow 5Li_2CuSn + Cu \quad (3)$$

$$12Li^+ + 5Li_2CuSn - 12e^- \Leftrightarrow 5Li_{4.4}Sn + 5Cu \quad (4)$$

Cu also buffers the volume change in active materials during the insertion/extraction of Li during the repeated charge/discharge processes because it does not form an alloy with Li. After the fifth cycle, the IRC value stops undergoing significant change and maintains in the low level.

The cyclic curve of the SnO surface-modified anode can be categorized in three regions (Figure 5d), related to the cyclic performance of the outmost SnO layer (zone I), middle Sn layer (zone II), and innermost Cu_6Sn_5 layer (zone III).[38] The

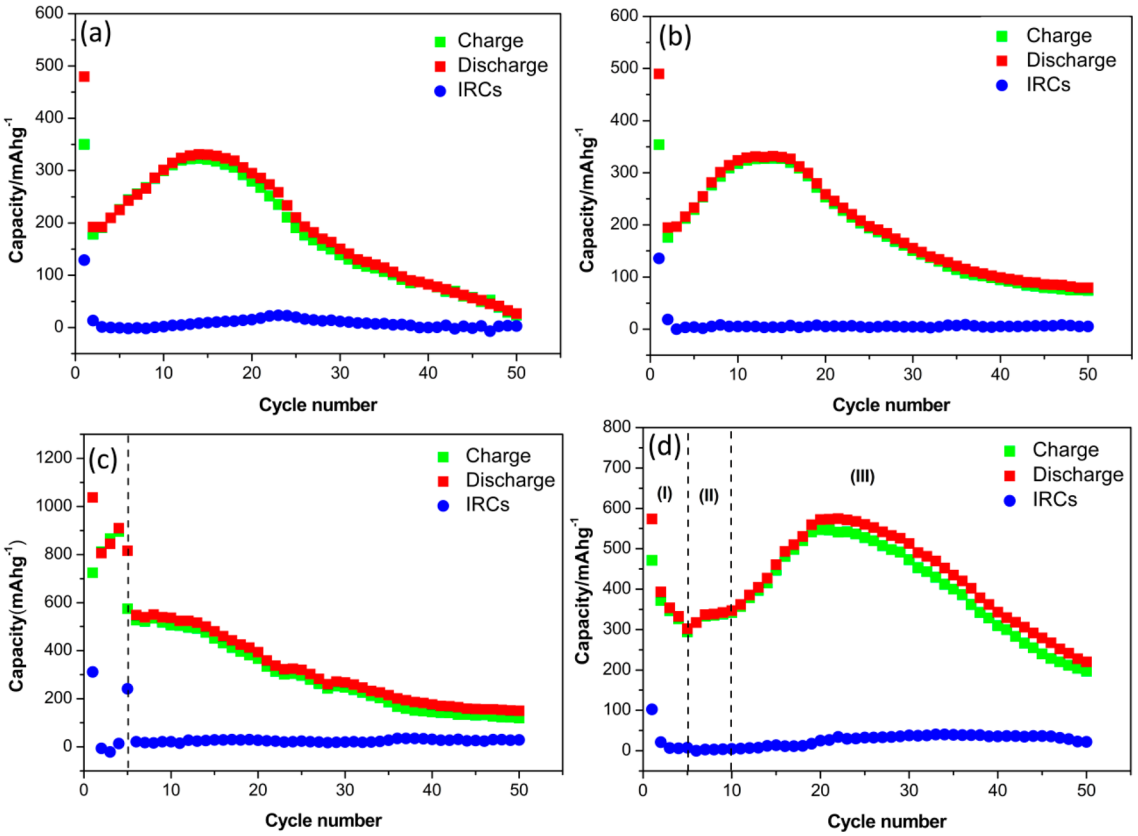

Figure 5. Cyclic performance of Sn-based film anodes treated under different conditions for Li ion cells: (a) as-electrodeposited, (b) sintered at 200 °C in argon for 12 h, (c) covered by Cu and sintered at 200 °C in argon for 12 h, and (d) sintered at 200 °C in air for 48 h.

middle Sn layer shows the maximum charge/discharge capacity of 342.5/347.2 mAh g^{-1} in the 10th cycle, which is comparable to that of the as-electrodeposited Sn anode (331.3/323.3 mAh g^{-1} in the 14th cycle, Figure 5a). The middle Sn layer also shows the smallest capacity and IRC, while the innermost Cu_6Sn_5 layer shows the highest value in capacity and IRC. The average IRC values of SnO (zone I), Sn (zone II), and Cu_6Sn_5 (zone III) are 6.9, 3, and 36 mAh g^{-1} respectively. The high IRC values of the Cu_6Sn_5 layer may be attributed to its defect structure formed via sintering during alloying between Cu and Sn.

Results shown above indicate that samples c and d with surface modification by Cu_6Sn_5 and SnO, respectively, have significantly different first cycle IRC values compared with the as-electrodeposited Sn anode (sample a), but they show unnoticeable change in first cycle IRC values and charge/discharge capacities of the anode after heat treatment in argon (sample b). Therefore, it is worth investigating the electrical resistance properties of the two modified anodes by electrochemical impedance spectrum (presented in Figure 6). The ac impedance spectrum of the as-electrodeposited anode and corresponding equivalent circuit are also presented in Figure 6. The equivalent circuit consists of the resistance of the electrolyte (R1), resistance/capacity of the SEI film (Rf/Cf), charge transfer resistance/double layer capacity (Rct/Cd), and Warburg impedance (Zw). Values of resistances Rf and Rct for the three Sn-based anodes are listed in Table 2. Notice that the as-electrodeposited Sn anode has the largest charge transfer resistance (140 Ω cm^2) due to the large obstruction of its thickest dense Sn film to the insertion of Li ions, resulting in the smallest charge/discharge capacity (350.5/479.6 mAh g^{-1}).

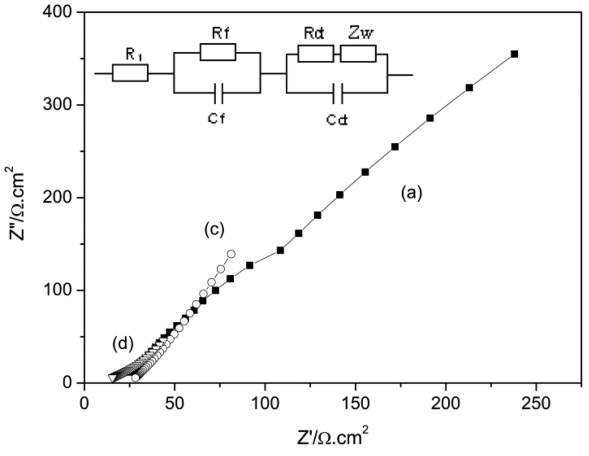

Figure 6. AC impedance spectra of the Sn-based anodes for Li ion cells: (a) as-electrodeposited, (c) covered by Cu and sintered at 200 °C in argon for 12 h, and (d) sintered at 200 °C in air for 48 h.

Table 2. Resistance of Charge Transfer and SEI Film of Sn-Based Anodes for Li Ion Batteries[a]

sample no.	a	c	d
Rf/Ω cm^2	15	135	4.5
Rct/Ω cm^2	140	9.8	25

[a](a) as electrodeposited, (c) covered by Cu and then sintered at 200 °C in argon for 12 h, and (d) sintered at 200 °C in air for 48 h.

The Cu_6Sn_5 surface-modified Sn anode shows the largest SEI film resistance (135 Ω cm^2) because of the large contacting

dx.doi.org/10.1021/sc500202m | ACS Sustainable Chem. Eng. 2014, 2, 1857−1863

surface with the electrolytes and large amount of defects, both of which are beneficial for formation of SEI films that leads to high IRC values of the anode.[10] The SnO surface-modified Sn anode (sample d) showed the lowest SEI film resistance, which is consistent with the conclusion obtained above that the presence of SnO can accelerate the insertion/extraction process of Li ions and decrease the IRC values of the cell. Because Warburg impedance in equivalent circuit reflects intrinsic resistances of the anodes and is presented by straight lines in the electrochemical impedance spectra in the low frequency range, it can also be observed that the as-electrodeposited Sn anode has the largest Warburg impedance, while the SnO surface-modified Sn anode has the smallest one, which is attributed to the thick Cu_6Sn_5 layer in the anode. Study of impedance spectra further revealed the relationship between the structure and properties of the Sn-based anodes.

CONCLUSIONS

Dense Sn-based anodes were prepared by pulse electrodeposition and post-heat-treated under different conditions for investigation of the influence of their surface structure on the charge/discharge capacity and IRC for Li ion batteries. The IRC values of all cycles and anodes are given with corresponding alloy/de-alloy reactions of various architectures analyzed in detail. The charge/discharge capacities and IRC values of the Sn-based anodes for Li ion batteries are shown to be strongly dependent on their surface morphology and composition. The as-electrodeposited Sn anode, composed of the thickest dense Sn film, demonstrated the smallest first cycle charge/discharge capacity and IRC as well as the largest charge transfer resistance. The Cu_6Sn_5 surface-modified Sn anode showed the largest first cycle charge/discharge capacity and the highest IRC as well as the largest SEI film resistance. Its charge/discharge capacity and IRC in the first cycle are 725/1036.7 and 311.7 mAh g^{-1}, respectively. The SnO surface-modified Sn anode had low SEI film resistance and the smallest IRC at the first cycle. The presence of SnO in the surface coating is preferable for a decrease in the first cycle IRC values, and defect is favorable for the IRC values. This work provides a fundamental understanding of the relationship between the first cycle charge/discharge capacity, IRC, and surface structure of Sn-based anodes of Li ion batteries for sustainable transfer of energy.

AUTHOR INFORMATION

Corresponding Authors

*E-mail: lilicmu@gmail.com, ll644@cornell.edu (L.L.). Tel: +1-412-482-8712 (L.L.).

*E-mail: slwang@mail.neu.edu.cn (S.W.).

Notes

The authors declare no competing financial interest.

ACKNOWLEDGMENTS

This work was supported by the National Natural Science Foundation of China No. 51274058.

REFERENCES

(1) Li, L.; Rohrer, G. S.; Salvador, P. A. Heterostructured ceramic powders for photocatalytic hydrogen production: Nanostructured TiO_2 shells surrounding microcrystalline (Ba,Sr)TiO_3 cores. *J. Am. Ceram. Soc.* **2012**, *95*, 1414−1420.

(2) Kamat, P. V. Meeting the clean energy demand: Nanostructure architectures for solar energy conversion. *J. Phys. Chem. C* **2007**, *111*, 2834−2860.

(3) Ramsurn, H.; Gupta, R. B. Nanotechnology in solar and biofuels. *ACS Sustainable Chem. Eng.* **2013**, *1*, 779−797.

(4) Li, L.; Salvador, P. A.; Rohrer, G. S. Photocatalysts with internal electric fields. *Nanoscale* **2014**, *6*, 24−42.

(5) Li, L.; Liu, X.; Zhang, Y.; Nuhfer, N. T.; Barmak, K.; Salvador, P. A.; Rohrer, G. S. Visible-light photochemical activity of heterostructured core-shell materials composed of selected ternary titanates and ferrites coated by TiO_2. *ACS Appl. Mater. Interfaces* **2013**, *5*, 5064−5071.

(6) Scrosati, B.; Garche, J. Lithium batteries: Status, prospects and future. *J. Power Sources* **2010**, *195*, 2419−2430.

(7) Karden, E.; Ploumen, S.; Fricke, B.; Miller, T.; Snyder, K. Energy storage devices for future hybrid electric vehicles. *J. Power Sources* **2007**, *168*, 2−11.

(8) Lopez, M. C.; Ortiz, G. F.; Lavela, P.; Alcantara, R.; Tirado, J. L. Improved energy storage solution based on hybrid oxide materials. *ACS Sustainable Chem. Eng.* **2013**, *1*, 46−56.

(9) Winter, M.; Besenhard, J. O.; Spahr, M. E.; Novak, P. Insertion electrode materials for rechargeable lithium batteries. *Adv. Mater.* **1998**, *10*, 725−763.

(10) Zhang, W.-J. A review of the electrochemical performance of alloy anodes for lithium-ion batteries. *J. Power Sources* **2011**, *196*, 13−24.

(11) Besenhard, J. O.; Yang, J.; Winter, M. Will advanced lithium-alloy anodes have a chance in lithium-ion batteries? *J. Power Sources* **1997**, *68*, 87−90.

(12) Park, C.-M.; Kim, J.-H.; Kim, H.; Sohn, H.-J. Li-alloy based anode materials for Li secondary batteries. *Chem. Soc. Rev.* **2010**, *39*, 3115−3141.

(13) Courtney, I. A.; Dahn, J. R. Electrochemical and in situ X-ray diffraction studies of the reaction of lithium with tin oxide composites. *J. Electrochem. Soc.* **1997**, *144*, 2045−2052.

(14) Idota, Y.; Kubota, T.; Matsufuji, A.; Maekawa, Y.; Miyasaka, T. Tin-based amorphous oxide: A high-capacity lithium-ion-storage material. *Science* **1997**, *276*, 1395−1397.

(15) Hu, R. Z.; Zeng, M. Q.; Zhu, M. Cyclic durable high-capacity Sn/Cu_6Sn_5 composite thin film anodes for lithium ion batteries prepared by electron-beam evaporation deposition. *Electrochim. Acta* **2009**, *54*, 2843−2850.

(16) Beaulieu, L. Y.; Eberman, K. W.; Turner, R. L.; Krause, L. J.; Dahn, J. R. Colossal reversible volume changes in lithium alloys. *Electrochem. Solid-State Lett.* **2001**, *4*, A137−A140.

(17) Uchiyama, H.; Hosono, E.; Honma, I.; Zhou, H.; Imai, H. A nanoscale meshed electrode of single-crystalline SnO for lithium-ion rechargeable batteries. *Electrochem. Commun.* **2008**, *10*, 52−55.

(18) Manthiram, A. Materials challenges and opportunities of lithium ion batteries. *J. Phys. Chem. Lett.* **2011**, *2*, 176−184.

(19) Kim, J. W.; Ryu, J. H.; Lee, K. T.; Oh, S. M. Improvement of silicon powder negative electrodes by copper electroless deposition for lithium secondary batteries. *J. Power Sources* **2005**, *147*, 227−233.

(20) Liu, J.; Li, W.; Manthiram, A. Dense core-shell structured SnO_2/C composites as high performance anodes for lithium ion batteries. *Chem. Commun.* **2010**, *46*, 1437−1439.

(21) Kim, H.; Choi, J.; Sohn, H.; Kang, T. The insertion mechanism of lithium into Mg_2Si anode material for Li-ion batteries. *J. Electrochem. Soc.* **1999**, *146*, 4401−4405.

(22) Wachtler, M.; Winter, M.; Besenhard, J. O. Anodic materials for rechargeable Li-batteries. *J. Power Sources* **2002**, *105*, 151−160.

(23) Ulus, A.; Rosenberg, Y.; Burstein, L.; Peled, E. Tin alloy-graphite composite anode for lithium-ion batteries. *J. Electrochem. Soc.* **2002**, *149*, A635−A643.

(24) Stjerndahl, M.; Bryngelsson, H.; Gustafsson, T.; Vaughey, J. T.; Thackeray, M. M.; Edstrom, K. Surface chemistry of intermetallic AlSb-anodes for Li-ion batteries. *Electrochim. Acta* **2007**, *52*, 4947−4955.

(25) Bryngelsson, H.; Stjerndahl, M.; Gustafsson, T.; Edstrom, K. How dynamic is the SEI? *J. Power Sources* **2007**, *174*, 970−975.
(26) Chang, K.; Wang, Z.; Huang, G.; Li, H.; Chen, W.; Lee, J. Y. Few-layer SnS_2/graphene hybrid with exceptional electrochemical performance as lithium-ion battery anode. *J. Power Sources* **2012**, *201*, 259−266.
(27) Zhou, X.; Wan, L.-J.; Guo, Y.-G. Binding SnO_2 nanocrystals in nitrogen-doped graphene sheets as anode materials for lithium-ion batteries. *Adv. Mater.* **2013**, *125*, 2152−2157.
(28) Ferguson, P. P.; Dunlap, R. A.; Dahn, J. R. An in situ study of the electrochemical reaction of li with nanostructured $Sn_{30}Co_{30}C_{40}$. *J. Electrochem. Soc.* **2010**, *157*, A326−A332.
(29) Matsuno, S.; Noji, M.; Kashiwagi, T.; Nakayama, M.; Wakihara, M. Construction of the ternary phase diagram for the Li-Cu-Sb system as the anode material for a lithium ion battery. *J. Phys. Chem. C* **2007**, *111*, 7548−7553.
(30) Li, H.; Shi, L.; Lu, W.; Huang, X.; Chen, L. Studies on capacity loss and capacity fading of nanosized SnSb alloy anode for Li-ion batteries. *J. Electrochem. Soc.* **2001**, *148*, A915−A922.
(31) Xu, K.; von Cresce, A. Interfacing electrolytes with electrodes in Li ion batteries. *J. Mater. Chem.* **2011**, *21*, 9849−9864.
(32) Wachtler, M.; Besenhard, J. O.; Winter, M. Tin and tin-based intermetallics as new anode materials for lithium-ion cells. *J. Power Sources* **2001**, *94*, 189−193.
(33) Mukaibo, H.; Osaka, T.; Reale, P.; Panero, S.; Scrosati, B.; Wachtler, M. Optimized Sn/SnSb lithium storage materials. *J. Power Sources* **2004**, *132*, 225−228.
(34) Wang, G.; Lu, Z. W.; Gao, X. P.; Liu, X. J.; Wang, J. Q. Electrochemical performance of La-Co-Sn alloys as anode materials for li-ion batteries. *J. Power Sources* **2009**, *189*, 655−659.
(35) Wang, C.; John Appleby, A.; Little, F. E. Electrochemical study on nano-Sn, $Li_{4.4}Sn$ and $AlSi_{0.1}$ powders used as secondary lithium battery anodes. *J. Power Sources* **2001**, *93*, 174−185.
(36) Wang, S.; Zhao, W.; Liu, X.; Li, L. Electrochemical performances of Cu_6Sn_5-modified sn anode with multi-layer structure for Li-ion cell. *RSC Adv.* **2013**, *3*, 18339−18344.
(37) Huang, Z.; Hu, S.; Hou, X.; Ru, Q.; Yu, H.; Zhao, L.; Li, W. Dead lithium phase investigation of Sn-Zn alloy as anode materials for lithium ion battery. *Chin. Sci. Bull.* **2009**, *54*, 1003−1008.
(38) Wang, S.; Zhao, W.; Wang, Y.; Liu, X.; Li, L. Characteristic performance of Sno/Sn/Cu_6Sn_5 three-layer anode for Li-ion battery. *Electrochim. Acta* **2013**, *109*, 46−51.
(39) Tamura, N.; Ohshita, R.; Fujimoto, M.; Fujitani, S.; Kamino, M.; Yonezu, I. Study on the anode behavior of Sn and Sn-Cu alloy thin-film electrodes. *J. Power Sources* **2002**, *107*, 48−55.
(40) Tu, K. N.; Thompson, R. D. Kinetics of interfacial reaction in bimetallic Cu-Sn thin films. *Acta Metall.* **1982**, *30*, 947−952.
(41) Patterson, A. L. The scherrer formula for X-ray particle size determination. *Phys. Rev.* **1939**, *56*, 978.
(42) Keller, R. M.; Baker, S. P.; Arzt, E. Quantitative analysis of strengthening mechanisms in thin Cu films: Effects of film thickness, grain size, and passivation. *J. Mater. Res.* **1998**, *13*, 1307−1317.
(43) Chung, S.-Y.; Bloking, J. T.; Chiang, Y.-M. Electronically conductive phospho-olivines as lithium storage electrodes. *Nat. Mater.* **2002**, *1*, 123−128.
(44) Islam, M. S.; Driscoll, D. J.; Fisher, C. A. J.; Slater, P. R. Atomic-scale investigation of defects, dopants, and lithium transport in the $LiFePO_4$ olivine-type battery material. *Chem. Mater.* **2005**, *17*, 5085−5092.
(45) Li, W.-Y.; Xu, L.-N.; Chen, J. Co_3O_4 nanomaterials in lithium-ion batteries and gas sensors. *Adv. Funct. Mater.* **2005**, *15*, 851−857.
(46) Foster, D. L.; Wolfenstine, J.; Read, J. R.; Behl, W. K. Nanocomposites of Sn and Li_2O formed from the chemical reduction of SnO as negative electrode material for lithium-ion batteries. *Electrochem. Solid-State Lett.* **2000**, *3*, 203−204.
(47) Li, H.; Shi, L.; Wang, Q.; Chen, L.; Huang, X. Nano-alloy anode for lithium ion batteries. *Solid State Ionics* **2002**, *148*, 247−258.
(48) Li, H.; Huang, X.; Chen, L.; Zhou, G.; Zhang, Z.; Yu, D.; Mo, Y. J.; Pei, N. The crystal structural evolution of nano-Si anode caused by lithium insertion and extraction at room temperature. *Solid State Ionics* **2000**, *135*, 181−191.
(49) Zhou, G. W.; Li, H.; Sun, H. P.; Yu, D. P.; Wang, Y. Q.; Huang, X. J.; Chen, L. Q.; Zhang, Z. Controlled Li doping of Si nanowires by electrochemical insertion method. *Appl. Phys. Lett.* **1999**, *75*, 2447−2449.
(50) Chiu, K. F.; Lin, H. C.; Lin, K. M.; Lin, T. Y.; Shieh, D. T. The significant role of solid oxide interphase in enhancement of cycling performance of Sn thin-film anodes. *J. Electrochem. Soc.* **2006**, *153*, A1038−A1042.
(51) Hu, R.; Liu, H.; Zeng, M.; Liu, J.; Zhu, M. Progress on Sn-based thin-film anode materials for lithium-ion batteries. *Chin. Sci. Bull.* **2012**, *57*, 4119−4130.
(52) Yang, J.; Takeda, Y.; Imanishi, N.; Yamamoto, O. Ultrafine Sn and $SnSb_{0.14}$ powders for lithium storage matrices in lithium-ion batteries. *J. Electrochem. Soc.* **1999**, *146*, 4009−4013.
(53) Yang, J.; Wachtler, M.; Winter, M.; Besenhard, J. O. Sub-microcrystalline Sn and Sn-SnSb powders as lithium storage materials for lithium-ion batteries. *Electrochem. Solid-State Lett.* **1999**, *2*, 161−163.
(54) Yang, J.; Takeda, Y.; Imanishi, N.; Xie, J. Y.; Yamamoto, O. Intermetallic $SnSb_x$ compounds for lithium insertion hosts. *Solid State Ionics* **2000**, *133*, 189−194.
(55) Fransson, L.; Nordstrom, E.; Edstrom, K.; Haggstrom, L.; Vaughey, J. T.; Thackeray, M. M. Structural transformations in lithiated η-Cu_6Sn_5 electrodes probed by in situ mossbauer spectroscopy and X-ray diffraction. *J. Electrochem. Soc.* **2002**, *149*, A736−A742.